Science Press

ARTICLE

Effect of Current Density on Micro-arc Oxidation Properties of TC11 Titanium Alloy

Yang Mei[1],   Tang Ning[1],   Chen Jin[2],   Huang Tingyu[1],   Yang Honglang[1],   Liu Yang[1],
Wang Dan[1],   Liu Wei[1]

[1] Southwest Petroleum University, Chengdu 610500, China; [2] Sichuan Oil and Gas Construction Engineering Company, Chengdu 610500, China

Abstract: The micro-arc oxidation coating was prepared on TC11 sample using sodium silicate (Na_2SiO_3) and sodium tungstate (Na_2WO_4) as electrolytes. Scanning electron microscopy (SEM), X-ray diffraction (XRD), and micro-hardness tester were used to analyze the coating surface and cross-sectional morphology and micro-hardness of the inner and outer ceramic coating. The results show that at 9 A/dm^2 current density, the optimal coating has an improved micro-hardness but the adhesion decreases compared to that of the pristine Ti substrate. The electrochemical corrosion and general corrosion of the coating were comparatively analyzed in 3.5% NaCl and 30% H_2SO_4 solution. When the current density is 9 A/dm^2, the coating obtained in the 30% H_2SO_4 solution has a lower self-corrosion current density. Finally, the wear mechanism of the coating was studied by the anti-wear experiment with SiC.

Key words: titanium alloy; micro-arc oxidation; wear resistance; corrosion resistance

TC11 titanium alloy is widely used in the aerospace, aviation and marine industry due to its light weight, high specific strength, specific stiffness, good thermal conductivity biocompatibility, etc[1-3]. However, the disadvantages of large friction coefficient, poor wear resistance and low hardness restrict the application of titanium and its alloys. To enhance the wear-resistance and corrosion-resistance of TC11 titanium alloy, many surface treatments have been proposed such as chemical conversion[4], anodic oxidation[5], physical chemical vapor deposition[6], plasma spraying[7], sol-gel deposition[8] and micro-oxidation (MAO). Micro-arc oxidation (MAO) is a new electrochemical metal surface treatment technique in recent years, which can in-situ grow porous ceramic membrane on the surface of non-ferrous metals, and realize the functional design of the membrane by changing the processing conditions and electrolyte composition[9-12]. It has attracted considerable interests due to high efficiency, energy saving and environmental protection for value metals such as Al, Ti, Mg and Nb as well as alloys, which have good wear resistance, corrosion resistance and photocatalytic perfor-

mance[13-15]. Herein, the purpose of this research is to investigate the variation law of voltage affected by current density in constant current mode, and the effect of current on surface and cross-section morphology, thickness, hardness and bonding force of coating. The friction characteristics of coating were studied, and the corrosion performance of the coating in 3.5% NaCl and 30% H_2SO_4 solution was discussed.

1 Experiment

The TC11 alloy (6.5 wt% Al, 0.5 wt% Zn, 3.3 wt% Mo, 0.25 wt% Si, and balance Al) with a dimension of Φ20 mm×3 mm was used as the substrate in the MAO process applied by Baoji Chenghui Titanium Industry Co., Ltd. The surface of substrates was polished successively with SiC papers up to 1000 grit, washed in ethanol and distilled water, and dried in a cool air prior to MAO. The electrolyte was prepared by dissolving 20 g/L sodium silicate (Na_2SiO_3) and 10 g/L sodium tungstate (Na_2WO_4) in distilled water. The prepared substrates were connected to anode and a stainless steel plate was used as the cathode in MAO. MAO was performed at a

constant duty cycle (15%) at 100 Hz for 20 min using a 20 kW AC power supply. The current density was fixed in a range of $3\sim12$ A/dm^2. The system was cooled by cold water pumped through double walls of the bath. After MAO, the samples were rinsed in distilled water and dried in air.

The phase composition of the treated surface was determined by X-ray diffraction (XRD) with a Cu target and the data were collected at $2\theta=10°\sim80°$ with a step size of $0.01°$. And the surface morphology of the samples was observed by scanning electron microscopy (SEM). In addition, the elemental composition of the treated surfaces was detected by an energy dispersive X-ray spectrometer (EDS). The thickness and surface Vickers hardness were measured on the coating thickness gauge (MC-2000A) and Vickers hardness tester (HVS-1000), respectively. The bonding strength of the coatings to substrate was tested by a multifunctional material surface property tester (MFT-4000). The brine immersion test was conducted on a precision salt spaying tester using 5% NaCl. The Tafel curves were acquired on the electrochemical workstation with 3.5% NaCl solution and 30% H$_2$SO$_4$ solution as the electrolyte. The test was performed between -1.5 V and 10 V versus saturated calomel electrode (SCE) at a scanning rate of 1 mV/s at room temperature. Friction and wear properties of TC11 titanium alloy and SiC balls were both examined using Swiss CSM ball-type friction and wear tester. The test was performed by reciprocating friction (with 1 N normal load and 30 s holding time). The surface roughness and wear scar depth and width were measured on the Ambios technology XP2 step meter.

2 Results and Discussion

Four samples were subjected to MAO in electrolytes prepared by dissolving 20 g/L sodium silicate (Na$_2$SiO$_3$) and 10 g/L sodium tungstate (Na$_2$WO$_4$) in distilled water at a current density of 3, 6, 9, and 12 A/dm^2 at 100 Hz, using a duty cycle of 15% for 20 min. Fig.1 shows the evolution of the micro-discharges and voltage with time. It shows that the sparking voltage increases with increasing the current density, The amount of heat released and generated increases with
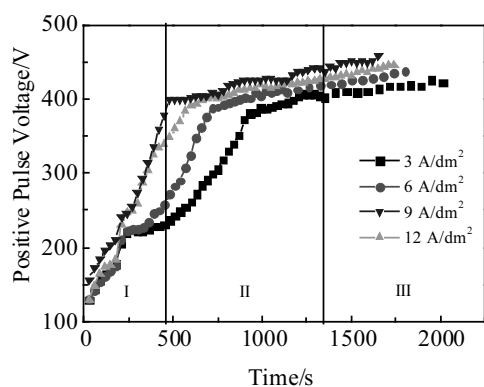
increasing the current density, which leads to the increase in formation speed and thickness of the coating, as well as the work required for the spark discharge to break through the coating, so the voltage becomes high.

The MAO process can be divided into three stages. In stage I, anodizing first occurs on the surface to form a thin passivation coating. In stage II, as the coating thickens, the resistance becomes larger and the voltage value increases. When the voltage increases to a certain value, the coating is broken down, and oxygen atoms are precipitated on the sample. Oxygen reacts with electrolyte particles to form a metal compound, which forms a surface coating after cooling. In stage III, as the thickness of the coating increases, the spark discharge becomes sparse, and click-through occurs where the coating is thinner. The growth of the coating changes from uniform growth to local growth, and the thickness of the coating and the voltage increase slowly.

The sample surface morphology at different current densities is displayed in Fig.2. There is a certain roughness on the surface of coating, which has a porous and loose structure with obvious melting marks and micro-cracks. As the current density increases, the surface roughness of coating and the pore size increase gradually, and the number of micro-pores decreases, so the surface of coating becomes rougher. The variation of surface morphology with current density can also be explained by the Keller model and the Ma Shengli correction model[16].

The cross-sectional morphology of the sample prepared at different current densities is presented in Fig.3. The thickness of the dense layer and the loose layer of the coating increases with increasing the current density, the overall thickness also increases, and the surface roughness of the coating increases remarkably.

Effect of current density on the Vickers hardness of the ceramic coating prepared at different current densities is shown in Fig.4. The average surface hardness of the coating increases with increasing the current density. It is attributed to the increase in the high hardness TiO$_2$ phase, which increases the coating thickness and the density of the inner coating. However, since the hardness of the base titanium alloy is low and the outermost layer of the coating is rough and porous, the hardness of the outermost layer of the coating is generally low.

The thickness and bonding force of the coatings prepared at different current densities are shown in Fig.5. With increasing the current density, the average surface thickness of the coating increases. The current density increases with increasing the oxidation rate of the metal surface, which accelerates the migration and deposition rate of the negatively charged colloidal particles in the oxidizing solution, and results in an increase in the growth rate of the coating, thereby obtaining a thicker coating. However, if the current density is too high, during the growth process of the micro-arc oxidation coating, it is easy to cause arcing, breakdown, foaming, etc[17]. The
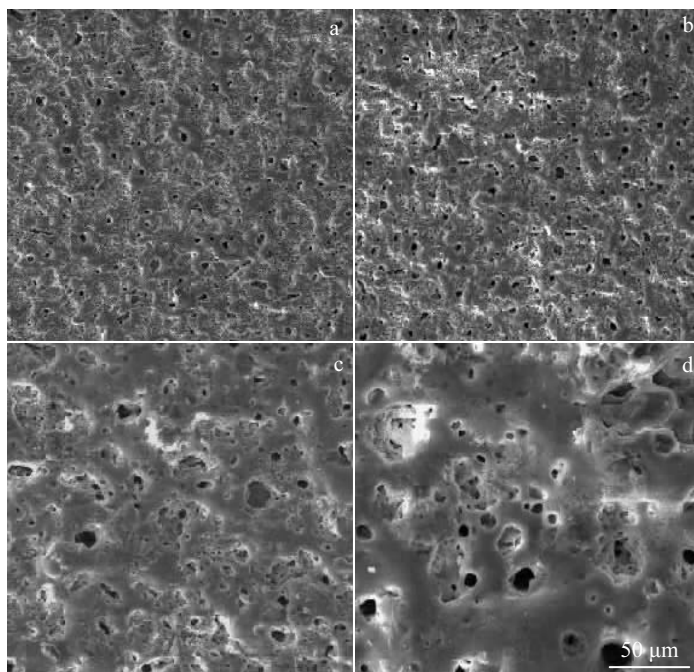

Fig.1　Voltage-time curves

Fig.2   SEM surface morphologies of the sample prepared at different current densities: (a) 3 A/dm^2, (b) 6 A/dm^2, (c) 9 A/dm^2, and (d) 12 A/dm^2
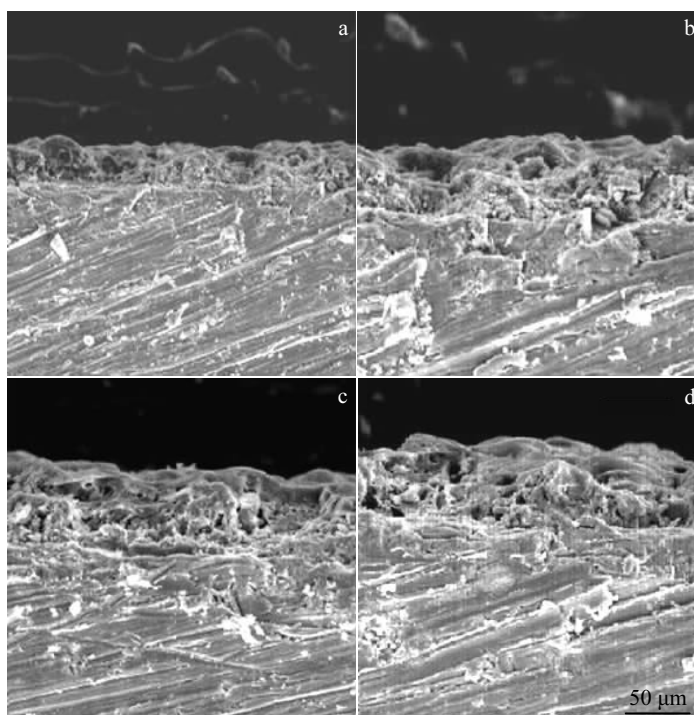

Fig.3   SEM cross-sectional morphologies of the sample prepared at different current densities: (a) 3 A/dm^2, (b) 6 A/dm^2, (c) 9 A/dm^2, and (d) 12 A/dm^2

adhesion force of the coating to the substrate decreases with increasing the current density. A possible explanation is that as the current density increases, the coating becomes thicker but the micro-pores on the surface coating decrease, and the macro-pores and the surface roughness increase, which leads to the formation of more micro-cracks and the increase in hardness
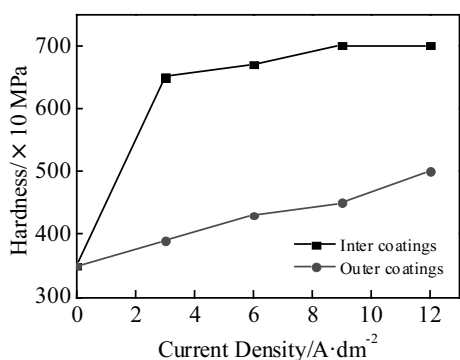
Fig.4   Hardness of the ceramic coatings prepared at different current densities
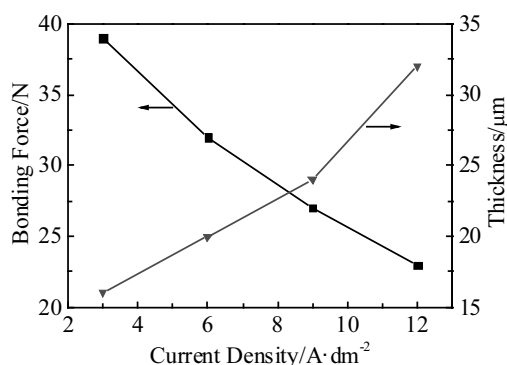

Fig.5   Thickness and bonding force of the MAO coatings prepared at different current densities

and brittleness of the coating. So the current density is generally selected to be about 9 A/dm^2.

XRD pattern of the MAO coating prepared at 9 A/dm^2 is presented in Fig.6, revealing TiO$_2$, γ-Al$_2$O$_3$ and Al$_2$TiO$_5$. No obvious α-Al$_2$O$_3$ peaks are found because the transformation of low temperature phase γ-Al$_2$O$_3$ into high temperature phase α-Al$_2$O$_3$ is inhibited[18]. The amount of rutile-TiO$_2$ is small, which is attributed to the fact that titanium dioxide can form
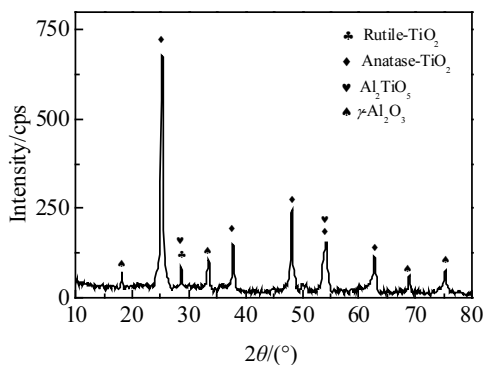

Fig.6   XRD pattern of the MAO coating prepared at 9 A/dm^2

metastable anatase-TiO$_2$ first and it is gradually converted into rutile-TiO$_2$. The MAO coating shows excellent corrosion resistance due to the formation of Al$_2$TiO$_5$ and TiO$_2$.

Fig.7a is the SEM cross-sectional morphology of the MAO coating prepared at 9 A/dm^2. The content of Ti and Al in the inner layer is high. However, no obvious Si element can be observed. The content of Si, W, O is gradually increased from the inner layer to the outermost layer due to the entry of elements. The XRD results indicate that many amorphous peaks are found on the surface coating. In addition, the EDS results indicate that there is Si on the surface, suggesting the existence of many amorphous phases SiO^2 in the coating[19]. The content of Ti and Al gradually decreases from the inner layer to the outermost layer, and Al is not identified on the coating due to its low content. The distribution of elements is closely related to the diffusion of elements in the oxidation process. Ti and Al diffuse and oxidize directly in the discharge channel, and the diffusion of Si and W in the coating is mainly along the discharge channel. During the spark discharge process, oxygen rapidly diffuses through the plasma discharge channel in the form of oxygenated ions and dissolved oxygen to the molten titanium alloy in the discharge region, which reacts at high temperature and high pressure to form titanium coating. With the action of the electric field, WO^{2-} and SiO^{2-} contact the surface of the titanium alloy through the discharge channel, and they are melted and solidified into the coating.

Fig.8 shows the counter-grinding test of TC11 titanium alloy and SiC sphere. The change of the coefficient of friction applied pressure is observed. At the beginning of the test, the coefficient of friction of the TC11 titanium alloy is approximately 0.24. When the number of rubbing reaches 200 r, the friction coefficient rapidly increases to about 0.46. After the number of revolutions exceeds 200 r, the coefficient of friction fluctuates around 0.46. The sample is not smooth and has a certain roughness, which leads to reduced actual contact area of the grinding.

The graph of the grinding mark step of the sample after rubbing is shown in Fig.9. The entire curve is bouncing up and down, because the scanned portion is rough and uneven. In the scanning interval of 0~1000 μm and 2000~3000 μm, the curve jump amplitude is relatively large, indicating that the surface roughness of the coating is large. When the scan is in the 1000~2000 μm interval, the curve has a certain jitter amplitude. The reason is that the structure of the coating is not uniform and the wear debris generated during the wear process makes the grinding mark uneven.

The model of the sliding friction and wear mechanism of the coated dome is shown in Fig.10. Fig.10a shows the morphology of the porous multi-volcanic reactor and ceramic particles on the coating surface. The MAO coating and SiC ball are in point contact, and the ceramic particles on the surface coating are first subjected to impact; the coating becomes sensitive under repeated impact and cracks appear,
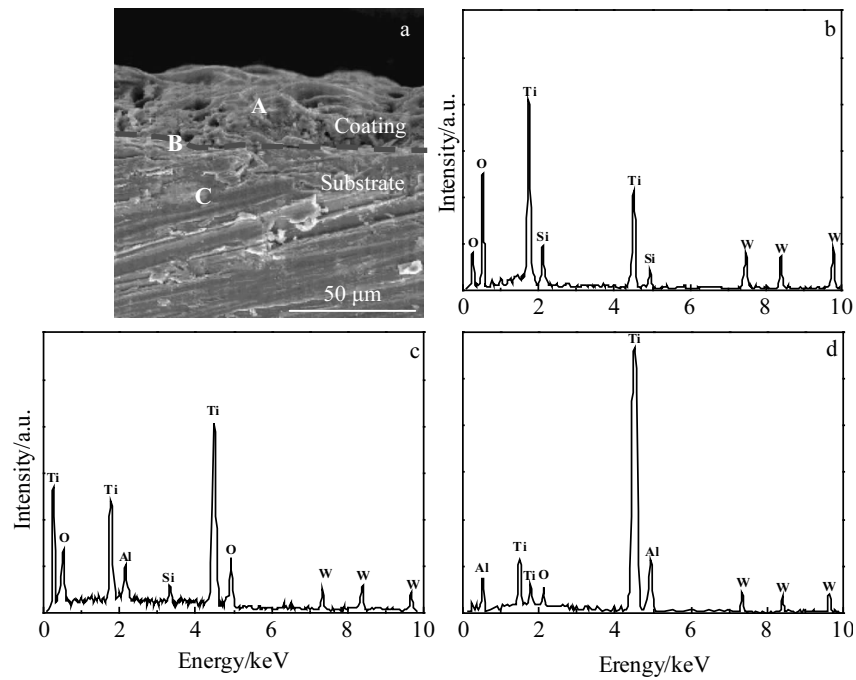
Fig.7   SEM cross-sectional morphology (a) of the 9 A/dm² MAO coating and EDS spectra of different regions marked in Fig.7a:
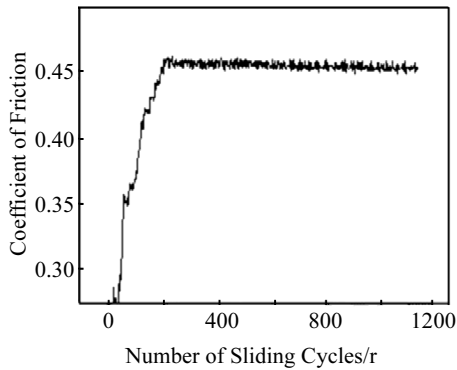(b) region A, (c) region B, and (d) region C

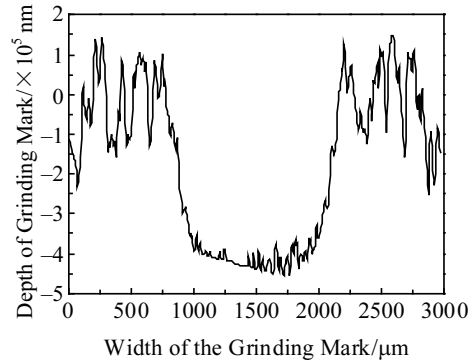Fig.8   Curve of friction coefficient of TC11 titanium alloy and
SiC sphere

Fig.9   Curve of the grinding mark step of TC11 and SiC on grinding
cycle

and the ceramic particles are quickly worn away, resulting in sharp ceramic fragments. The small holes on the surface coating are where the crack stress is concentrated, and the coating is broken by large stress; the broken pieces and particles are piled up to form wear debris into the friction contact surface, deposited in the grinding mark or scattered in the pores of the coating, as shown in Fig.10b. When the grinding debris accumulates to a certain amount, it will cause three-body wear. Due to the high hardness of the coating and the rough surface, the wear ball has a certain degree of wear during the wear process, and the presence of furrows can be observed after the SiC ball test. The ploughed abrasive chips

may stick to the coating surface and change the friction type. That is, the friction between pure SiC and ceramic coating becomes mixed friction, and the wear mode changes from particle wear to particle wear and mixed wear of adhesive wear and particle wear. Therefore, it is necessary to polish the coating before the abrasion. The polishing treatment removes ceramic particles protruding from the surface coating, as shown in Fig.10c. There are still many voids on the surface of coating after polishing, which lead to the entering of generated fine debris. After the grinding debris fills the pores, the residue deposits on the contact surface, as shown in Fig.10d. The friction will be hindered by the wear debris and change

the friction condition and friction coefficient.

The potentiodynamic polarization curves measured after immersing the substrate and 9 A/dm^2 MAO samples in a neutral 3.5% NaCl and 30% H$_2$SO$_4$ solution for 1 h are shown in Fig.11. Fig.11a is consistent with Fig.11b, both suggesting that the coated samples show higher positive corrosion potentials than the substrate, and indicating better anti-corrosion performance[20,21]. Treated sample's self-corrosion current density is reduced relative to untreated sample, suggesting a good resistance to uniform corrosion. The main reason for the good corrosion resistance of the coating in Fig.11a is the increase of the corrosion resistant phase TiO. Fig.11b shows that the corrosion current is reduced by 3 orders of magnitude compared to untreated samples.

The morphologies of selected samples (pristine Ti, 9 A/dm^2 MAO coating) after the brine immersion test with 5% NaCl and 30% H$_2$SO$_4$ solution are shown in Fig.12. Fig.12b shows that the pristine sample in 5% NaCl solution is corroded obviously with a large corrosion pit on the surface. It may be attributed to the fact that Cl$^-$ has a strong penetrating ability and can penetrate the coating to corrode[22]. After the MAO coating is corroded in 5% NaCl, the surface corrosion is weakened, which shows that the corrosion resistance is improved, as shown in Fig.12e. Fig.12c shows that lots of corrosion pits can be observed from the pristine Ti corroded in 30% H$_2$SO$_4$ solution, while no obvious corrosion pits can be seen from the MAO coating shown in Fig.12f. All above suggests that the dense MAO coating offers effective
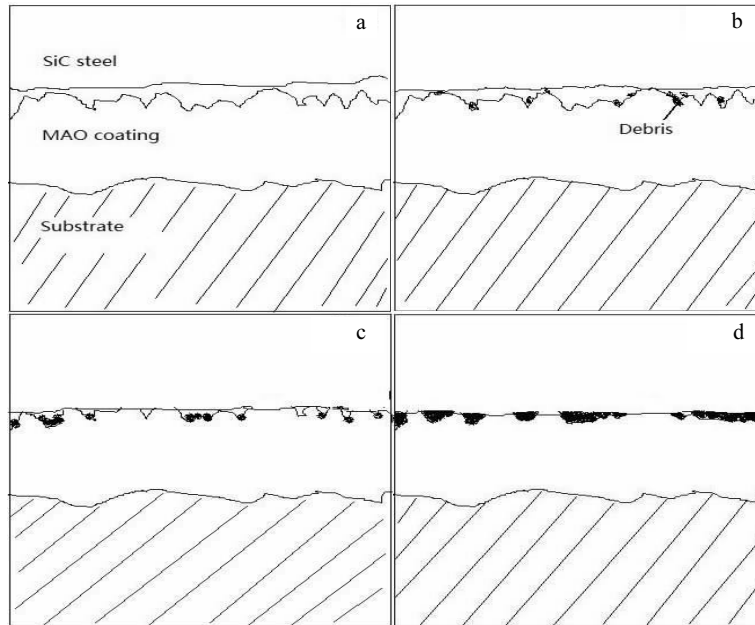

Fig.10   Model of sliding friction and wear mechanism of coating ball plate: (a) surface coating consisting of porous multi-volcanic piles and ceramic particles; (b) grinding debris deposited in wear scar or scattered in micro-pores; (c) polishing before wear; (d) wear debris deposited on the contact surface
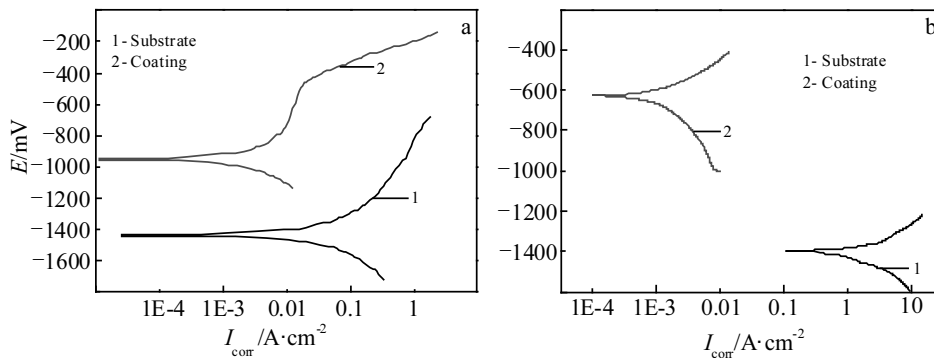

Fig.11   Potentiodynamic polarization curves of pristine and 9 A/dm^2 MAO coating immersed in different corrosive agents: (a) 3.5% NaCl solution and (b) 30% H$_2$SO$_4$ solution
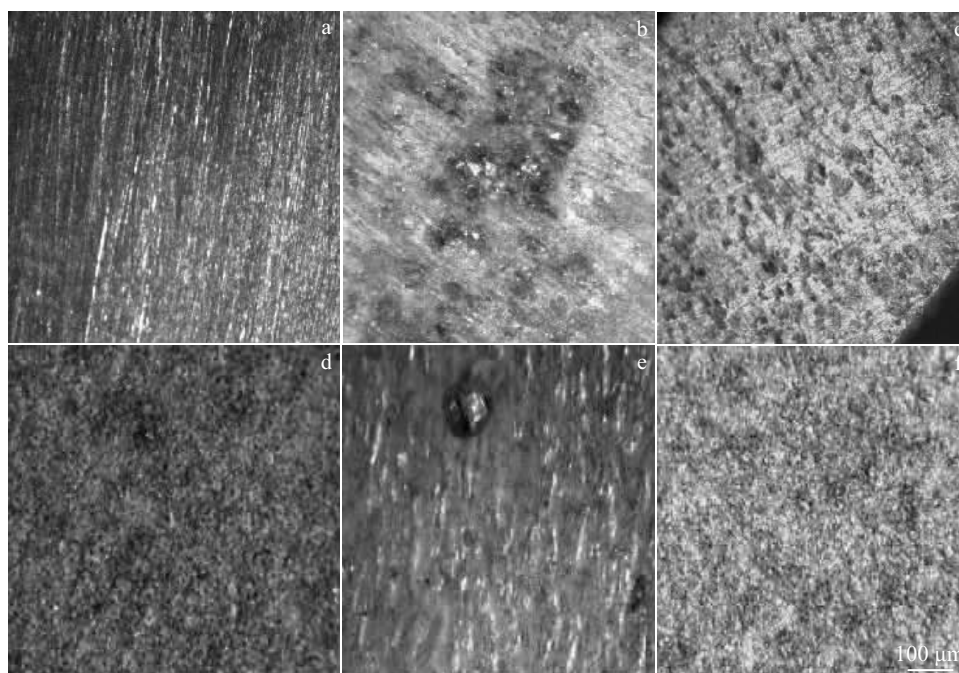
Fig.12   Morphologies of substrate sample and micro-arc oxidation coating before and after corrosion: (a) substrate, (b) substrate in 5% NaCl, and
(c) substrate in 30% H_2SO_4; (d) MAO coating, (e) MAO coating in 5% NaCl, and (f) MAO coating in 30% H_2SO_4

protection against corrosion for Ti alloy.

3   Conclusions

1) A compact ceramic coating with different current densities can be prepared on the TC11 titanium alloy by micro-arc oxidation (MAO) method in an electrolyte composed of sodium silicate (Na_2SiO_3) and sodium tungstate (Na_2WO_4).

2) The optimal coating with 9 A/dm^2 current density has an improved micro-hardness but the adhesion decreases compared to the pristine Ti substrate.

3) The friction characteristics in the MAO titanium alloy are proposed. When the current density is 9 A/dm^2, the self-corrosion current density of coating obtained in the 30% H_2SO_4 solution is reduced by 3 orders of magnitude compared to that of the untreated samples, which is consistent with the result from the brine immersion test, suggesting the excellent corrosion resistance of the MAO coating.

References

1   Morais L S, Serra G G, Muller C A. *Acta Biomater*[J], 2007, 3: 331

2   Xue W, Krishna B V, Bandyopadhyay A. *Acta Biomater*[J], 2007, 3: 1007

3   Diego S B, Micéli G B, Segattomello D. *Revista Odonto Ciencia*[J], 2011, 26: 209

4   Valdez B, Kiyota S, Stoytcheva M *et al*. *Corrosion Science*[J], 2014, 87(5): 141

5   Mei Y, Tingyu H, Dan W *et al*. *Transactions of the IMF*[J], 2018, 96(5): 269.

6   Zhang Q, Leng Y, Xin R. *Biomaterials*[J], 2005, 26(16): 2857

7   Kossenko A, Lugovskoy S, Astashina N et al. *Glass Physics & Chemistry*[J], 2013, 39(6): 639

8   Hasannejad H, Shahrabi T, Rouhaghdam A S *et al*. *Appl Surf Sci*[J], 2008, 254: 5683

9   Cui X, Kim H M, Kawashita M *et al*. *Journal of Materials Science*[J], 2008, 19(4): 1767

10   Zhu X, Ong J L, Kim S *et al*. *Journal of Biomedical Materials Research*[J], 2002, 60(2): 333

11   Abbasi S, Rezaie H R, Golestani-Fard F. *Characterization and Development of Bio-systems and Biomaterials*[J], 2013, 29: 227

12   Jin F, Chu P K, Wang K *et al*. *Materials Science & Engineering*[J], 2008, 476(1-2): 78

13   Yerokhin A L, Nie X, Leyland A *et al*. *Surf Coat Tech*[J], 1999, 122: 73

14   Sah S P, Tsuji E, Aoki Y *et al*. *Corros Sci*[J], 2012, 55: 90

15   Cui L Y, Zeng R C, Guan S K *et al*. *J Alloy Compd*[J], 2017, 695: 2464

16   Zhang X, Du J, Liu B *et al*. *Journal of Materials Research*[J], 2007, 22(9): 2497

17   Yan J K, Teng Y, Ni E X *et al*. *Key Engineering Materials*[J], 2016, 697: 612

18   Wu Zhendong, Jiang Zhanhua, Yao Zhongping. *Chinese Journal of Nonferrous Metals*[J], 2005, 5(6): 946

19   Wang Yaming, Jiang Ailing, Guo Lixin. *Chinese Journal of Nonferrous Metals*[J], 2004, 14(4): 548

20　Mohedano M, Matykina E, Arrabal R *et al. Applied Surface Science*[J], 2015, 346: 57

21　Yang W, Li Q, Qian X *et al. Progress in Organic Coatings*[J],

2015, 89: 260

22　Gu Y, Cai X, Guo Y *et al. Materials & Design*[J], 2013, 43: 542

电流密度对 TC11 钛合金微弧氧化性能的影响

杨　眉[1]，唐　宁[1]，陈　劲[2]，黄婷玉[1]，杨洪浪[1]，刘　洋[1]，王　丹[1]，刘　伟[1]

(1. 西南石油大学，四川 成都 610500)

(2. 四川石油天然气建设工程有限公司，四川 成都 610500)

摘　要：以硅酸钠（Na_2SiO_3）和钨酸钠（Na_2WO_4）为电解质在 TC11 钛合金表面生成一层微弧氧化膜。使用扫描电子显微镜（SEM）、X 射线衍射仪（XRD）和显微硬度测试仪等观察涂层表面形貌和横截面形貌以及内外陶瓷膜层的显微硬度。结果表明，与基体钛合金相比，当电流密度为 9 A/dm^2，膜层的显微硬度得到提高，但附着力有所降低。 此外，在 3.5% NaCl 和 30% H_2SO_4 溶液中比较分析了膜层的电化学腐蚀和一般腐蚀，当电流密度为 9 A/dm^2 时，在 30% H_2SO_4 溶液中的膜层具有较低的自腐蚀电流密度。最后，通过 SiC 和膜层的对磨实验研究了膜层的磨损机理。

关键词：钛合金；微弧氧化；耐磨性；耐腐蚀性能

作者简介：杨　眉，男，1971 年生，博士，副教授，西南石油大学材料科学与工程学院，四川 成都 610500，电话：028-83037416，E-mail: meiyangs0099@163.com